Heliyon 7 (2021) e08087

Contents lists available at ScienceDirect

Heliyon

journal homepage: www.cell.com/heliyon

Research article

Influence of iron binding in the structural stability and cellular internalization of bovine lactoferrin

Caroline Augusto Barros [a], Daniel Sanches [b], Carlos Alberto Marques de Carvalho [c], Ronimara Aparecida Santos [d], Theo Luiz Ferraz de Souza [e], Vitor Luis Macena Leite [a], Samir Pereira da Costa Campos [f], Andréa Cheble de Oliveira [f], Rafael Braga Gonçalves [a,*]

[a] Departamento de Bioquímica, Instituto Biomédico, Universidade Federal do Estado do Rio de Janeiro, 20211-040, Rio de Janeiro, RJ, Brazil
[b] Natural Sciences Department, Arts and Sciences Division, South Florida State College, 33825, Avon Park, FL, United States
[c] Departamento de Patologia, Centro de Ciências Biológicas e da Saúde, Universidade do Estado do Pará, 66095-662, Belém, PA, Brazil
[d] Departamento de Nutrição Básica e Experimental, Instituto de Nutrição, Universidade do Estado do Rio de Janeiro, 20550-900, Rio de Janeiro, RJ, Brazil
[e] Faculdade de Farmácia, Universidade Federal do Rio de Janeiro, 21941-590, Rio de Janeiro, RJ, Brazil
[f] Instituto de Bioquímica Médica Leopoldo de Meis, Instituto Nacional de Ciência e Tecnologia de Biologia Estrutural e Bioimagem, Universidade Federal do Rio de Janeiro, 21941-902, Rio de Janeiro, RJ, Brazil

ARTICLE INFO

Keywords:
Bioactive component
Denaturation
Fluorescence spectroscopy
Functionality
Guanidine hydrochloride
Lactoferrin
Microscopy

ABSTRACT

Lactoferrin (Lf) is an iron-binding glycoprotein and a component of many external secretions with a wide diversity of functions. Structural studies are important to understand the mechanisms employed by Lf to exert so varied functions. Here, we used guanidine hydrochloride and high hydrostatic pressure to cause perturbations in the structure of bovine Lf (bLf) in apo and holo (unsaturated and iron-saturated, respectively) forms, and analyzed conformational changes by intrinsic and extrinsic fluorescence spectroscopy. Our results showed that the iron binding promotes changes on tertiary structure of bLf and increases its structural stability. In addition, we evaluated the effects of bLf structural change on the kinetics of bLf internalization in Vero cells by confocal fluorescence microscopy, and observed that the holo form was faster than the apo form. This finding may indicate that structural changes promoted by iron binding may play a key role in the intracellular traffic of bLf. Altogether, our data improve the comprehension of bLf stability and uptake, adding knowledge to its potential use as a biopharmaceutical.

1. Introduction

Lactoferrin (Lf) is a high-affinity iron-binding protein found in milk, semen, mucosal secretions, saliva and tears (Wang et al., 2017). Many biological functions attributed to Lf have been extensively demonstrated, of which can be highlighted the immunomodulatory, anti-inflammatory, antitumor, antiviral, cell growth-stimulating and antioxidant activities (Carvalho et al., 2017; Hering et al., 2017; Cutone et al., 2017; Lizzi et al., 2009; Luzi et al., 2017). Previous studies showed that Lf can be effective *in vitro* against infection by several virus species, such as Herpes simplex, Influenza A, Dengue, Zika, Chikungunya, Mayaro, Sindbis and Semliki forest viruses (Marchetti et al., 2004; Waarts et al., 2005; Carvalho et al., 2014, 2017; Chen et al., 2017; Superti et al., 2019), in addition to Severe acute respiratory syndrome (SARS) pseudovirus (Lang et al., 2011). Besides, recent studies have also pointed out Lf as a potential antiviral agent for treatment of coronavirus disease 2019 (COVID-19) (Carvalho et al., 2020; Mirabelli et al., 2020; Chang et al., 2020; Kell et al., 2020; Peroni and Fanos, 2020; AlKhazindar and Elnagdy, 2020). In the last twenty years, publications on Lf increased by more than 40% compared to the period from 1960 to 1999.

The three-dimensional structure of Lf is comprised of a single polypeptide chain of 76 kDa divided into two lobes (C and N), linked by an alpha helix, with two domains in each lobe (C1/C2 and N1/N2) (Moore et al., 1997). The protein has one iron-binding site in each lobe and an affinity for this ion 260 times greater than that of transferrin (Baker et al., 1994). Its iron-saturated form is called holo-Lf, while the unsaturated form is called apo-Lf. Lf not only binds Fe^{2+} and Fe^{3+} ions, but also other metal ions such as Cu^{+2}, Mn^{+2} and Zn^{+2} (Baker et al., 2004).

Despite the large number of studies exploring the structural properties of Lf, little is known about the stability of this protein (Schwarcz

* Corresponding author.
E-mail address: rafael.braga@unirio.br (R.B. Gonçalves).

https://doi.org/10.1016/j.heliyon.2021.e08087
Received 24 May 2021; Received in revised form 20 August 2021; Accepted 26 September 2021

et al., 2008; Bokkhim et al., 2013; Franco et al., 2013; Sreedhara et al., 2010; Wakabayashi et al., 2008). Since the functions performed by Lf depend on its correct three-dimensional structure, it is important to uncover the factors that can affect this property. Ion binding is known to lead to protein structural stabilization (Jancsó et al., 2011; Bai et al., 2010; Puri et al., 2015), generating multiple interactions between amino acids that participate in the anchoring of these ions. The investigation of the role of iron binding is of utmost relevance to a proper comprehension of the functionality of Lf.

Moreover, the three-dimensional structure of proteins can be further influenced by physical factors such as temperature and pressure, leading to loss of biological activity (Cao et al., 2018; Franco et al., 2018; Silva et al., 2014; Akazawa-Ogawa et al., 2017; Sreedhara et al., 2010; Patel et al., 2006; Privalov, 2009). High hydrostatic pressure (HHP) has been widely used to study the thermodynamics of protein folding and protein–protein or protein–nucleic acid interactions (Silva et al., 2014; Cordeiro et al., 2013; Torrent et al., 2004; Balny et al., 2002). HHP causes a slight perturbation in protein structure, affecting the tenuous balance between stabilization and destabilization of the many interactions that occur in the molecule (Mozhaev et al., 1994). The major advantage of using HHP over high temperature to study protein stability is the induction of less drastic structural changes (Perrett and Zhou, 2002). As a chemical approach, the use of denaturing agents such as guanidine hydrochloride (GnHCl) is also relevant, since transitions between protein conformations and other parameters such as organization and aggregation can be addressed (Syed et al., 2018; Anumalla and Prabhu, 2018; Niether et al., 2018; Bian and Ji, 2014). Therefore, the use of these structure-disrupting agents coupled with the possibility of monitoring the transition process between the native and unfolded states is useful to assess the difference in structural stability of apo and holo-bLf – i.e., the role of iron in the structure of this protein.

In this work, we aimed at investigating the influence of iron ions in the structural stability of bovine Lf (bLf), by subjecting both apo and holo-bLf to physical and chemical agents while monitoring protein conformational changes by spectroscopic techniques. In addition, using confocal fluorescence microscopy, we also evaluated the role of iron binding on the *in vitro* cellular internalization of bLf.

2. Results

2.1. Chemical denaturation of bLf is decreased by iron binding

We used increasing GnHCl concentration to promote structural changes and access the fully unfolded state of apo- and holo-bLf. Based on intrinsic fluorescence emission by tryptophan residues, we found that initial spectral center of mass values for apo- and holo-bLf were 29,510 ± 44 and 29,165 ± 9 cm^{-1} (p value = 0.0058), respectively (Figure 1), indicating that tryptophan in holo-bLf is more exposed to the solvent than in apo-bLf. A gradual increase in GnHCl concentration led to an abrupt denaturation in apo-bLf, while holo-bLf denaturation level was approximately linear with GnHCl concentration. At the final GnHCl concentration of 7 M, apo and holo-bLf reached a common denaturation endpoint. However, the GnHCl concentration required to bring apo and holo-bLf to 50% denaturation ($G_{1/2}$) was 2.75 M and 3.5 M, respectively (inset in Figure 1). The same denaturation profile was observed using urea to disturb the bLf structure (data not shown).

To confirm the effect of GnHCl on bLf structure, we next used the hydrophobic probe bis-ANS (4,4′-bis-1-anilinonaphthalene-8-sulfonate) (Figure 2). As shown, apo-bLf bound more efficiently to this probe than holo-bLf, especially at lower GnHCl concentrations (up to 3 M) (p value <0.001). Such a differential bis-ANS binding indicates that there are more structured hydrophobic regions exposed in apo-bLf than in holo-bLf. Differences in the denaturation of apo and holo-bLf were observed when binding to bis-ANS was decreased. Denaturation of apo-bLf compared to control was significant from 4 M GnHCl, while for holo-bLf such a value was 5 M.

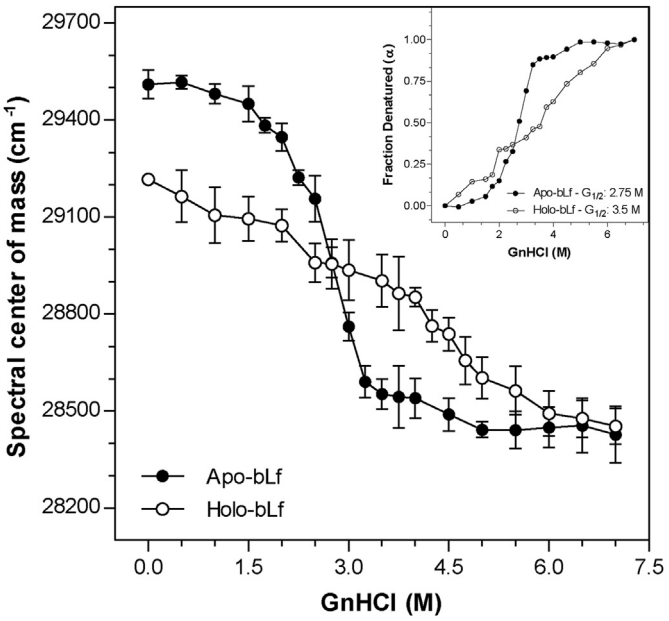

Figure 1. GnHCl-induced denaturation of bLf monitored using intrinsic fluorescence emission. In order to verify the effects of GnHCl and to obtain total denaturation of bLf, increasing concentrations of the compound was added to the protein (0.5 M–7.0 M). The protein was diluted in standard buffer to a final concentration of 500 μg/mL. The spectral center of mass was measured at various GnHCl concentrations. Fluorescence excitation wavelength: 280 nm; emission wavelength range: 300 nm–420 nm. The inset represents the denatured fraction of apo- and holo-bLf in the presence of GnHCl. Data were obtained from three independent experiments and plotted as mean ± SD. Differences in means compared to control were not significant up to 2 M GnHCl for holo-bLf and up to 1.5 M GnHCl for apo-bLf. For all other conditions, differences from the respective controls were significant. Student's t-test showed that the difference between apo- and holo-bLf at 0 M GnHCl was significant (p value = 0.0058).

2.2. Iron binding turns bLf more resistant to physical denaturation

HHP changes system volume by disrupting hydrophobic interactions in the protein core and promoting less dramatic changes in protein structure when compared with GnHCl denaturation. Our results showed that HHP appears to be more effective in causing structural disturbances in apo-bLf than in holo-bLf, as assessed by measuring spectral center of mass from intrinsic fluorescence emission (Figure 3). Protein unfolding was partially reversible for apo and no significant differences were observed for holo-bLf upon returning to atmospheric pressure.

To obtain a more pronounced pressure-denaturation of bLf, we also combined HHP with a subdenaturing GnHCl concentration (2 M). A synergism between HHP and GnHCl was observed under this condition, since deviations from the spectral center of mass of apo- and holo-bLf were 884 ± 68 cm^{-1} and 335 ± 109 cm^{-1}, respectively (Figure 3). As observed, refolding was partial for apo-bLf in the presence of GnHCl (2 M) and total for holo-blf when returned to normal conditions. This finding further demonstrated that apo- and holo-bLf are different as to structural stability, thus confirming the stabilizing role played by iron ions in the protein.

2.3. Denaturation of bLf affects binding but not retention of iron ions

By measuring iron absorbance at 465 nm, we next assayed how stable exogenous iron ions – in the form of the iron complex Fe(III)-nitrilotriacetic acid (Fe-NTA) – bind to bLf upon denaturation by increasing GnHCl concentration (Figure 4). Even at GnHCl concentrations as low as 1.5 M, apo-bLf had its ability to anchor iron ions affected, losing almost completely this property from 4.5 M GnHCl. On the other hand, iron retention by holo-bLf was almost unaffected even at GnHCl

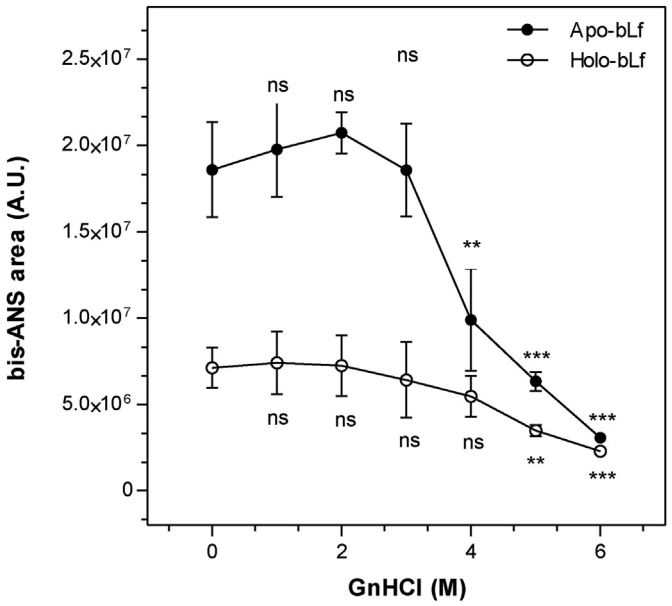

Figure 2. GnHCl-induced denaturation of bLf monitored using extrinsic bis-ANS fluorescence emission. The hydrophobic bis-ANS probe was used to monitor the denaturation of apo- and holo-bLf in the presence of GnHCl. The bis-ANS concentration used was 40 μM. The protein was diluted in standard buffer to a final concentration of 500 μg/mL. Fluorescence excitation wavelength: 360 nm; emission wavelength range: 400 nm–600 nm. Data were obtained from three independent experiments and plotted as mean ± SD. One-way ANOVA revealed significant differences in means compared to the respective controls, as shown in the figure (***, $p \leq 0.001$; **, $p \leq 0.01$; *, $p \leq 0.05$; ns = not significant, $p > 0.05$). Student's t-test showed differences in means of binding to bis-ANS between apo and holo-bLf, in control condition (p value = 0.0364).

concentrations as high as 4.5 M, and a significant decrease in retention of these ions was observed at 6 M GnHCl. As expected, iron content of holo-bLf did not change with addition of Fe-NTA.

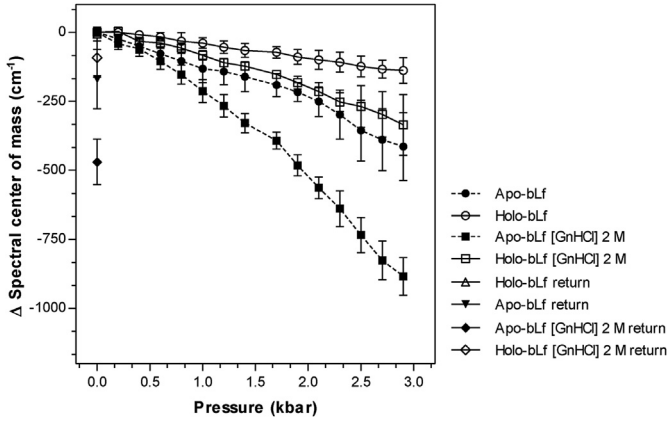

Figure 3. Pressure stability of bLf. Pressure stability of apo- and holo-bLf incubated or not with 2 M GnHCl was monitored by intrinsic fluorescence emission. The measured values of spectral center of mass after return to atmospheric pressure are denoted as "return". The protein was diluted in standard buffer to a final concentration of 500 μg/mL. Data were obtained from three independent experiments and plotted as mean ± SD. Differences in means compared to control were not significant for holo- and apo-bLf up to 0.8 kbar, apo-bLf [GnHCl] 2 M up to 0.4 kbar and holo-bLf [GnHCl] 2 M up to 1 kbar. Differences in spectral center of mass upon return to atmospheric pressure was not significant for holo-bLf and holo-bLf [GnHCl] 2 M compared to control condition at 0 kbar ($p > 0.05$). For apo-bLf and apo-bLf [GnHCl] 2 M the return had a significant difference of spectral center of mass in relation to the control ($p \leq 0.05$ and $p \leq 0.001$, respectively).

2.4. Iron binding accelerates the internalization of bLf in Vero cells

Given the differences in structural stability between apo- and holo-bLf observed by spectroscopic analysis, we decided to verify the influence of iron binding on bLf internalization in the Vero cells. Initially, colorimetric MTT (3-(4,5-dimethyl-2-thiazolyl)-2,5-diphenyl-2H-tetrazolium bromide) test was used to assess possible cytotoxic effects of bLf on Vero cells. By incubating the cells with a range of concentrations of apo- or holo-bLf, we observed that both forms of bLf were non-cytotoxic at concentrations up to 2 mg/mL (Figure 5). Based on this finding, bLf concentration used for the following experiments was 1 mg/mL.

To assess the internalization kinetics of the protein, Vero cells were incubated with fluorescein isothiocyanate (FITC)-labeled apo- or holo-bLf for 0, 30 and 60 min (Figure 6). Time zero represents the synchronization step, when bLf is bound to the cells at low temperature (4 °C) and hence there is no internalization. By raising temperature to 37 °C, the internalization process can occur. Using confocal fluorescence microscopy, we observed that internalization of apo- and holo-bLf had already occurred at 30 min post-binding. Although both forms were internalized, holo-bLf seemed to perform this task more quickly, since it was observed to accumulate in the perinuclear region at 60 min post-binding, when only a discrete fraction of apo-bLf had reached such a location.

3. Discussion

In this work, we compared the structural stability of apo- and holo-bLf by fluorescence spectroscopy and their cellular internalization by confocal fluorescence microscopy, demonstrating that iron binding improves both properties. We used guanidine hydrochloride, which is a salt used as a potent denaturing agent (Mason et al., 2007), and HHP, which induces water to enter the hydrophobic cavities of the protein (Silva et al., 2001) and has been increasingly used for food preservation and hygiene as an alternative to replace heat treatment (Munizaga et al., 2014; Franco et al., 2013; Aubourg et al., 2013).

It has been reported that metal ions can alter the structure and functionality of proteins, especially if it is an intrinsically disordered protein (IDP) (Jancsó et al., 2011). Since proteins are dynamic molecules, the binding of these ions can influence their structure in order to increase stability against some types of denaturing agents. GnHCl is a chaotropic agent that affects non-covalent bonds, disrupting the structure of water and, consequently, disrupting hydrophobic interactions that are fundamental for the maintenance of the tertiary structure of proteins. Our results using GnHCl showed that holo-bLf has a higher stability against chemical denaturation than apo-bLf (Figure 1). There is a conformational difference between iron-saturated and unsaturated forms of the protein (Baker et al., 2004). The iron binding induces the Lf structure to a more closed form as the domains attach to anchor this ion. In this way, iron increases the stability of the protein since its structure becomes more rigid and less susceptible to denaturation (Gerstein et al., 1993; Baker and Baker, 2008).

Apo-Lf has a more open and dynamic structure than holo-Lf, being more flexible, less stable, and more prone to thermal denaturation and proteolysis (Baker and Baker, 2008). These data also corroborate our findings on bLf denaturation assessed by bis-ANS, an extrinsic fluorescent probe that binds to hydrophobic segments exposed to solvent (Figure 2). Here, we showed that apo-bLf can bind more to this probe than holo-bLf and, with increasing GnHCl concentration, there is an increase in exposure of protein hydrophobic segments and consequently an increase in the intensity of bis-ANS fluorescence. Stanciuc et al. (2013) showed that gradual temperature rising also significantly increases ANS binding to Lf, and a study by Sreedhara et al. (2010) showed that an increase in ANS binding to Lf also occurs when Lf is subjected to pH values less than 5. In addition, we observed the stabilizing effect of iron by preventing the exposure of structured hydrophobic sites to bis-ANS in holo-bLf. This reinforces the difference between the three-dimensional structures of apo and holo forms of the protein and the stabilizing role of the iron ion.

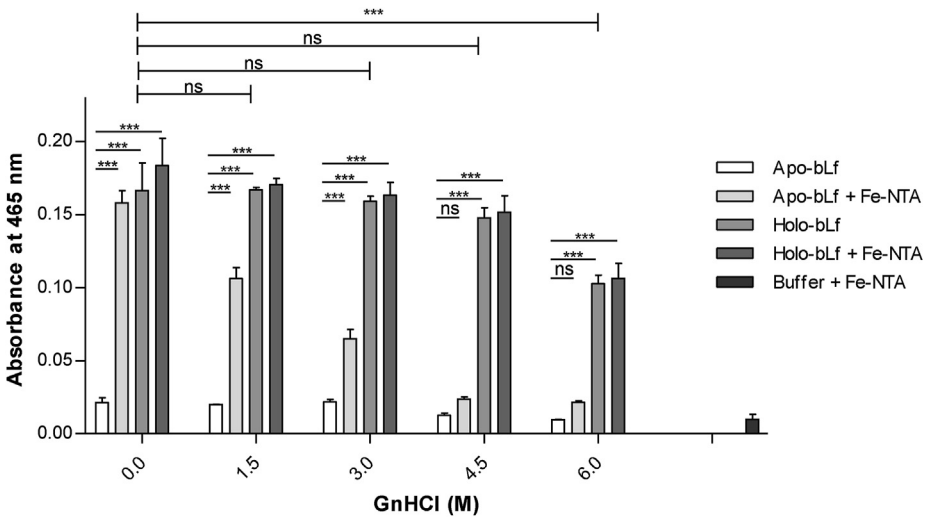

Figure 4. Quantification of iron in bLf under denaturing conditions. The quantification of iron in the apo- and holo-bLf structures was performed to evaluate the release of this ion in the presence of GnHCl with absorbance measurements at 465 nm. The protein was diluted in standard buffer to a final concentration of 3.5 mg/mL. Fe-NTA solution was added to the samples at 50 μM. Data were obtained from three independent experiments and plotted as mean ± SD. Statistical significance of differences in means compared to respective control conditions without iron, and comparison between holo-bLf under different GnHCl conditions are shown in the figure (***, $p \leq 0.001$; **, $p \leq 0.01$; *, $p \leq 0.05$; ns = not significant, $p > 0.05$).

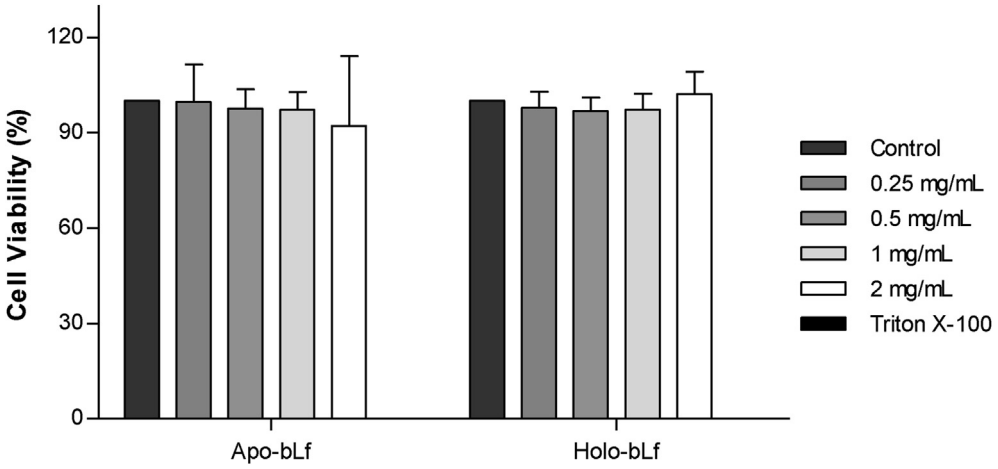

Figure 5. Cytotoxicity of bLf. In order to verify the cytotoxic effect of bLf (apo and holo) treatment on Vero cells, different concentrations of this protein were used (0.25, 0.5, 1 and 2 mg/mL). The negative control represents cells not treated with bLf and the positive control cells treated with 0.1% Triton X-100. Data points represent the average of three independent measurements. Only the difference in mean of Triton X-100 compared to control was significant ($p \leq 0.001$).

The use of HHP in combination to a subdenaturing GnHCl concentration to cause perturbations in the bLf structure gave us important information about the differences in stability between its apo and holo forms. We observed that holo-bLf presents a greater structural stability facing this treatment than apo-bLf since it has a lower variation of its spectral center of mass (Figure 3). A study conducted by Franco et al. (2013) showed that holo-bLf is more resistant to high pressure than apo-bLf. Our results showed that, in addition of the gain of stability, iron binding leads to a change in the tertiary structure of bLf. Previous studies showed through another spectroscopic technique, circular dichroism (CD), that the tertiary structure of bLf is affected by iron binding (Bokkhim et al., 2013). On the other hand, other studies indicate that there are no differences in the secondary structure between these two forms of bLf (Brown and Parry, 1974; Bokkhim et al., 2013). Differently from what is published in the literature, our work has comparatively shown the structural stability of both apo- and holo-bLf using fluorescence spectroscopy to monitor the entire unfolding process.

Lf has the ability to retain iron and this can be quantified through spectrophotometric analysis. Iron quantification can be performed using an absorption coefficient measured at 465 nm (Majka et al., 2013). Our result showed that holo-bLf did not fully release the iron ions from its structure even at high GnHCl concentrations such as 6 M (Figure 4). Using the HHP and temperature, Franco et al. (2013) verified that bLf maintains its ability to bind iron ions when subjected to a pressure of 400 MPa, with this phenomenon occurring much less significantly at 5 and 6 kbar. However, binding of iron ions to bLf was impaired using treatments such as 72 °C for 15 s. In a study conducted by Mata et al. (1998), recombinant human Lf with less than 18% iron saturation was shown to aggregate under heat treatment at 72 °C or 135 °C for 60 s, while still retaining the ability to bind iron ions. We have shown that, at low GnHCl concentrations, the iron binding site of apo-bLf already begins a process of unfolding. Nevertheless, once anchored in the bLf structure, the iron ions do not release completely, even at high GnHCl concentrations.

Lf is a multifunctional protein, and its strong antiviral activity has been reported for several DNA and RNA viruses such as Herpes, Zika, Chikungunya, BK and Hantavirus, among others (Marchetti et al., 1996, 1999; Murphy et al., 2000, 2001; Longhi et al., 2006; Carvalho et al., 2014, 2017). Some studies have demonstrated through *in vitro* and *in silico* models the activity of Lf against Severe Acute Respiratory Syndrome Coronavirus 2 (SARS-CoV-2), the causative agent of COVID-19 (Hu et al., 2021; Campione et al., 2021; Carvalho et al., 2020). As for other viruses (Carvalho et al., 2014; Waarts et al., 2005; Marchetti et al., 1996), *in vitro* inhibition of coronavirus infection by Lf appears to depend on the interaction of this protein with heparan sulfate proteoglycans (HSPGs), which serve as anchors to help virus binding to the cell surface (Hu et al., 2021; Lang et al., 2011). The cell line commonly used for antiviral assays

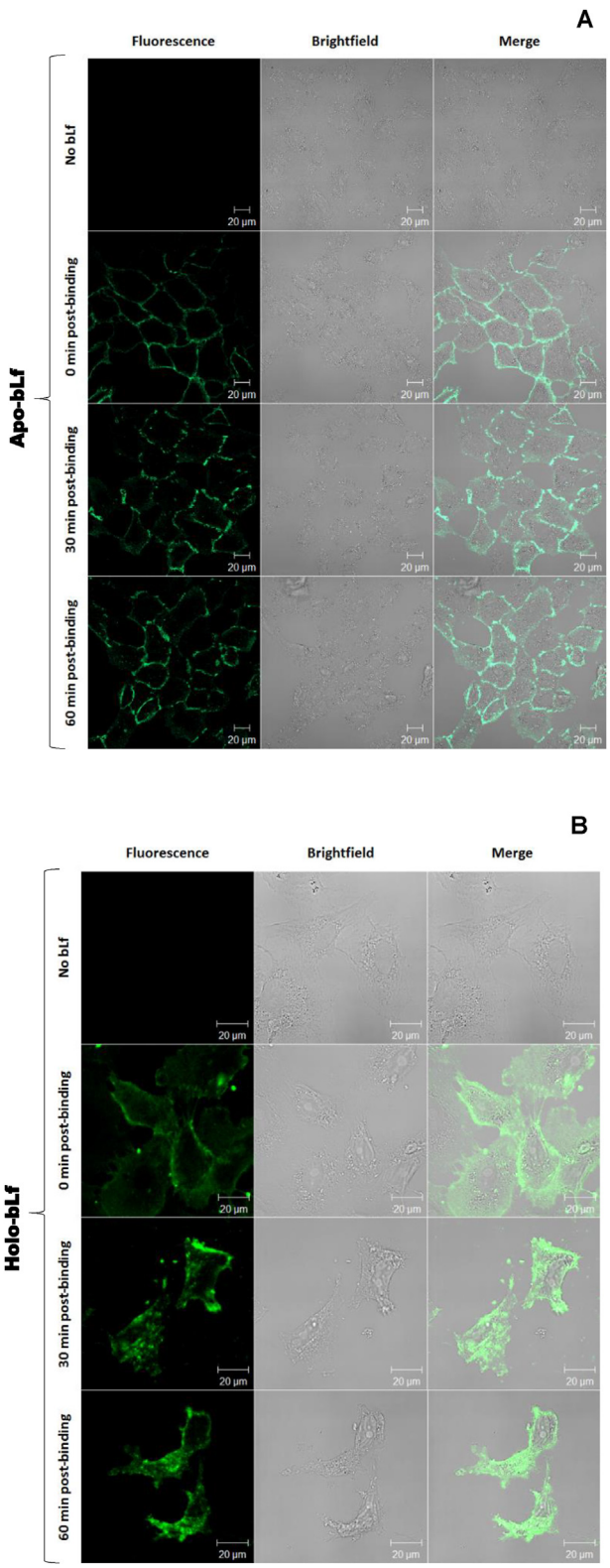

Figure 6. Internalization of bLf in Vero cells. BLf in its apo (A) or holo (B) forms were conjugated to FITC and synchronously incubated with Vero cells for 0, 30 or 60 min. BLf internalization was observed by laser-scanning confocal fluorescence microscopy. The selected groups of cells are representative of their respective open fields. White bars: 20 µm.

with Lf is Vero cells, which we used herein to investigate the internalization kinetics of apo- and holo-bLf.

Our results showed remarkable differences between apo- and holo-bLf regarding their internalization kinetics in Vero cells, but a lack of significant cytotoxicity for both forms (Figures 5 and 6). This may reflect distinct affinities of iron-free and iron-saturated forms of this protein to its specific receptor (LfR) present in this cell lineage, resulting in differential receptor-mediated endocytosis. Intriguingly, both apo- and holo-Lf were previously shown to enter Caco-2 cells via a similar mechanism, but no significant differences were observed for binding and uptake of apo- and holo-Lf in this cell lineage (Jiang et al., 2011). The endocytic uptake of Lf seems to be cholesterol-dependent and results in its partition into early endosomes and endoplasmic reticulum in the macrophage-like human THP-1 cells (Florian et al., 2012). Lf may even be targeted to the nucleus in the intestinal epithelial cell line Caco-2 (Ashida et al., 2004), where its internalization relies on the N1 domain of the protein (Suzuki et al., 2008). Therefore, it is important to further investigate the internalization routes of apo- and holo-bLf in these cells, which can consequently differentiate response mechanisms and potentially involved cellular pathways.

The internalization of Lf into cells may be important for its function. Oral administration of Lf has low absorptivity and the protein can be further degraded in the gastrointestinal tract, resulting in low bioavailability. The use of Lf as a nanocarrier has been studied because, in addition to being a multifunctional molecule, it can carry hydrophobic drugs that have low absorption and mediate the cellular internalization of these compounds (Singh et al., 2015; Liu et al., 2018; Sabra and Agwa, 2020). Serrano et al. (2020) showed the use of lactoferrin syrup in liposomal form (32 mg), vitamin C (12 mg) and zinc (10 mg) for the treatment of 75 patients diagnosed with COVID-19. According to this study, all patients recovered from symptoms within 4–5 days of treatment. Thus, studies of enhancement of Lf absorption and internalization mechanisms are important to improve its action on cellular targets (Serrano et al., 2020).

Finally, the presence of iron ions in the bLf structure turns the protein into a more stable conformation that lead to a more rapidly internalization when compared to the unsaturated form. Therefore, future studies aiming to further understand the role of iron ions in the cellular internalization of bLf are needed to provide a better comprehension of the mechanisms involved in its cellular responses.

4. Materials and methods

4.1. Chemicals

All reagents were of analytical grade. Distilled water was filtered and deionized. Apo-bLf was purchased from Life Extension (Fort Lauderdale, FL, USA). GnHCl, bis-ANS and Fe-NTA were purchased from Sigma-Aldrich (Saint Louis, MO, USA). The experiments were performed at 25 °C in a standard buffer comprised of 25 mM Tris and 150 mM NaCl at pH 7.5.

4.2. Preparation of apo- and holo-bLf

Apo-bLf was dissolved to a concentration of 100 mg/mL in phosphate-buffered saline (PBS) and centrifuged at 6,000 rpm for 5 min at 4 °C to remove the cellulose excipient. The supernatant was passed through a 0.22-mm syringe-driven filter unit (Millipore, Billerica, MA, USA), aliquoted and stored as a stock solution at 4 °C until further use. Holo-bLf was obtained from apo-bLf (10 mg/mL) diluted in 10 mM Tris and 75 mM NaCl, pH 7.2. FeNTA solution – 9.9 mM $Fe(NO_3)_3$ and 8.5 mM nitrilotriacetic acid, pH 7.0 – was added to apo-bLf in 2:1 proportion. To remove excess of iron ions from the solution, instead of water, the sample was dialyzed against the standard buffer described above at 4 °C for 48 h (Bokkhim et al., 2013; van Berkel et al., 1995). Both apo-bLf, holo-bLf was filtered, aliquoted and stored at 4 °C until further use.

4.3. Chemical denaturation

bLf was incubated with increasing concentrations of GnHCl (0.5–7 M) and allowed to equilibrate overnight prior to analysis. The protein was diluted into the standard buffer to a final concentration of 500 μg/mL. Each experiment was performed at least three times.

4.4. HHP and fluorescence spectroscopy

The high pressure bomb, described by Paladini and Weber (1981), was purchased from ISS (Champaign, IL, USA). Fluorescence spectra were recorded on an ISS K2 spectrofluorometer (ISS). Pressure was increased in steps of 0.2 kbar until 2.9 kbar. The samples were allowed to equilibrate for 10 min prior to measurements. For intrinsic fluorescence measurements, the tryptophan residues were excited at 280 nm and emission was observed from 300 to 420 nm. Changes in fluorescence spectra at pressure p were evaluated by changes in the spectral center of mass, $<\upsilon_p>$:

$$<\upsilon_p> = \Sigma \upsilon_i F_i / \Sigma F_i \quad (1)$$

where F_i stands for the fluorescence emitted at wavenumber υ_i and the summation is carried out over the range of appreciable values of F. Additionally, the extrinsic fluorescence measurement was performed using bis-ANS. In this case, the sample was excited at 360 nm and emission was observed from 400 to 600 nm. Unless otherwise stated, experiments were performed at 25 °C in standard buffer. Each experiment was performed at least three times.

4.5. Quantification of iron release

To verify the iron binding capacity of bLf in the presence of GnHCl, we used the spectrophotometer Multiskan GO (Thermo Scientific, Waltham, MA, USA). The samples were diluted in standard buffer and measured at 465 nm according to Franco et al. (2013). These experiments were done in triplicate with different preparations of bLf.

4.6. Cell culture

African green monkey kidney (Vero) cells were cultured as monolayers at 37 °C in a humidified atmosphere with 5% CO_2, using Dulbecco's modified Eagle's medium (DMEM) (Sigma-Aldrich) supplemented with 10% fetal bovine serum (Cultilab, Campinas, SP, Brazil) and 1% penicillin-streptomycin (Gibco, Grand Island, NY, USA).

4.7. Cytotoxicity assay

Vero cell monolayers seeded in 96-well plates (Costar, Corning, NY, USA) were incubated with different concentrations of bLf at 37 °C for 24 h and then assayed for MTT reduction for 3 h as previously described by Mosmann (1983).

4.8. Cellular internalization kinetics

Apo- and holo-bLf were incubated with FITC (Molecular Probes, Eugene, OR, USA) at a molar ratio of 1:10 in basic phosphate buffer (2.5% $Na_2HPO_4.7H_2O$ and 0.082% NaH_2PO_4 at pH 8.0) for 1 h at 4 °C. The unincorporated dye was removed by centrifuging through an Amicon Ultra filter unit with a 30 kDa molecular weight cut-off (Millipore). Labeled protein molecules were suspended in PBS, passed through a 0.22 mm syringe-driven filter unit and immediately used for experiments. FITC labeling was confirmed by subjecting the protein sample to sodium dodecyl sulfate-polyacrylamide gel electrophoresis (SDS-PAGE) followed by ultraviolet transillumination of the gel (Carvalho et al., 2014). Subconfluent Vero cells in 35 mm glass-bottom dishes (MatTek, Ashland, MA, USA) were incubated with 1 mg/mL FITC-labeled apo- or holo-bLf for 15 min at 4 °C to allow for bLf binding only. Unbound bLf molecules were washed away with ice-cold PBS and cells were immediately incubated with DMEM alone at 37 °C to allow for bLf internalization. At 0, 30 and 60 min post-binding, cells were washed with warm PBS and fixed with 3.7% formaldehyde in PBS for 15 min at room temperature. Samples were then visualized on a LSM 510 META laser-scanning confocal fluorescence microscope (Carl Zeiss, Oberkochen, BW, Germany) with excitation by an argon ion laser at 488 nm and emission collected from 500 to 550 nm using a plan-apochromat 63x/1.4 oil immersion objective. Pinhole aperture was adjusted to detect the fluorescence from an optical slice of 3 μm along the axial plane.

4.9. Statistical analyses

One-way ANOVA with Dunnett's post-test and Student's t-test were used to compare differences between groups. These analyses were made using Prism 6 software (GraphPad, San Diego, CA, USA). Data were expressed as mean ± SD, and statistically significant p-values (***, $p \leq 0.001$; **, $p \leq 0.01$; *, $p \leq 0.05$) were considered.

Declarations

Author contribution statement

Caroline Augusto Barros: Conceived and designed the experiments; Performed the experiments; Analyzed and interpreted the data; Wrote the paper.

Daniel Sanches: Performed the experiments; Analyzed and interpreted the data.

Carlos Alberto Marques de Carvalho: Conceived and designed the experiments; Performed the experiments; Analyzed and interpreted the data; Wrote the paper.

Ronimara Aparecida Santos: Performed the experiments.

Theo Luiz Ferraz de Souza: Conceived and designed the experiments; Analyzed and interpreted the data; Wrote the paper.

Vitor Luis Macena Leite: Performed the experiments.

Samir Pereira da Costa Campos: Conceived and designed the experiments; Analyzed and interpreted the data; Wrote the paper.

Andréa Cheble de Oliveira: Conceived and designed the experiments; Analyzed and interpreted the data; Contributed reagents, materials, analysis tools or data.

Rafael Braga Gonçalves: Conceived and designed the experiments; Analyzed and interpreted the data; Contributed reagents, materials, analysis tools or data; Wrote the paper.

Funding statement

This work was supported by the National Council for Scientific and Technological Development (CNPq) (to A.C.O) and Fundação Carlos Chagas Filho de Apoio a Pesquisa do Estado do Rio de Janeiro (FAPERJ) (to A.C.O. and R.B.G).

Data availability statement

Data included in article/supplementary material/referenced in article.

Declaration of interests statement

The authors declare no conflict of interest.

Additional information

No additional information is available for this paper.

References

Akazawa-Ogawa, Y., Nagai, H., Hagihara, Y., 2017. Heat denaturation of the antibody, a multi-domain protein. Biophys. Rev. 1–4.

AlKhazindar, M., Elnagdy, S.M., 2020. Can lactoferrin boost human immunity against COVID-19? Pathog. Glob. Health 1–2.

Anumalla, B., Prabhu, N.P., 2018. Glutamate induced thermal equilibrium intermediate and counteracting effect on chemical denaturation of proteins. J. Phys. Chem. B 2018 122 (3), 1132–1144.

Ashida, K., Sasaki, H., Suzuki, Y.A., Lönnerdal, B., 2004. Cellular internalization of lactoferrin in intestinal epithelial cells. Biometals 17 (3), 311–315.

Aubourg, S.P., Torres, J.A., Saraiva, J.A., Guerra-Rodrigues, E., 2013. Effect of high-pressure treatment applied before freezing and frozen storage on the functional and sensory properties of Atlantic mackerel (Scomber scombrus). LWT - Food Sci. Technol. (Lebensmittel-Wissenschaft -Technol.) 53, 100–106.

Bai, X., Teng, D., Tian, Z., Zhu, Y., Yang, Y., Wang, J., 2010. Contribution of bovine lactoferrin inter-lobe region to iron binding stability and antimicrobial activity against Staphylococcus aureus. Biometals 23 (3), 431–439.

Baker, E.N., Baker, H.M., 2008. A structural framework for understanding the multifunctional character of lactoferrin. Biochimie 91 (1), 3–10.

Baker, E.N., Anderson, B.F., Baker, H.M., Day, C.L., Haridas, M., Norris, G.E., Rumball, S.V., Smith, C.A., Thomas, D.H., 1994. Three-dimensional structure of lactoferrin in various functional states. Adv. Exp. Med. Biol. 1–12.

Baker, H.M., Anderson, B.F., Baker, E.N., 2004. Dealing with iron: common structural principles in proteins that transport iron and heme. Proc. Natl. Acad. Sci. U.S.A. 100, 3579–3583.

Balny, C., Masson, P., Heremans, K., 2002. High pressure effects on biological macromolecules: from structural changes to alteration of cellular processes. Biochim. Biophys. Acta Protein Struct. Mol. Enzymol. 1595 (1-2), 3–10.

Bian, L., Ji, X., 2014. Distribution, transition and thermodynamic stability of protein conformations in the denaturant-induced unfolding of proteins. PloS One 9 (3), e91129.

Bokkhim, H., Bansal, N., Grøndahl, L., Bhandari, B., 2013. Physico-chemical properties of different forms of bovine lactoferrin. Food Chem. 141, 3007–3013.

Brown, E.M., Parry, R.M., 1974. Spectroscopic study of bovine lactoferrin. Biochemistry 13 (22), 4560–4565.

Campione, E., Lanna, C., Cosio, T., Rosa, L., Conte, M.P., Iacovelli, F., Romeo, A., Falconi, M., Del Vecchio, C., Franchin, E., Lia, M.S., Minieri, M., Chiaramonte, C., Ciotti, M., Nuccetelli, M., Terrinoni, A., Iannuzzi, I., Coppeda, L., Magrini, A., Bernardini, S., Sabatini, S., Rosapepe, F., Bartoletti, P.L., Moricca, N., Di Lorenzo, A., Andreoni, M., Sarmati, L., Miani, A., Piscitelli, P., Valenti, P., Bianchi, L., 2021. Lactoferrin against SARS-CoV-2: in vitro and in silico evidences. Front. Pharmacol. 12, 666600.

Cao, B., Fang, L., Liu, C., Min, W., Liu, J., 2018. Effects of high hydrostatic pressure on the functional and rheological properties of the protein fraction extracted from pine nuts. Food Sci. Technol. Int. 24 (1), 53–66.

Carvalho, C.A.M., Sousa, I.P., Silva, J.L., Oliveira, A.C., Gonçalves, R.B., Gomes, A.M.O., 2014. Inhibition of Mayaro virus infection by bovine lactoferrin. Virology 452–453, 297–302.

Carvalho, C.A.M., Casseb, S.M.M., Gonçalves, R.B., Silva, E.V.P., Gomes, A.M.O., Vaconcelos, P.F.C., 2017. Bovine lactoferrin activity against Chikungunya and Zika viruses. J. Gen. Virol. 98 (7), 1749–1754.

Carvalho, C.A.M., Matos, A.R., Caetano, B.C., Junior, I.P.S., Campos, S.P.C., Geraldino, B.R., Barros, C.A., Almeida, M.A.P., Rocha, V.P., Silva, A.M.V., Melgaço, J.G., Neves, P.C.C., Barros, T.A.C., Ano Bom, A.P.D., Siqueira, M.M., Missailidis, S., Gonçalves, R.B., 2020. Vitro Inhibition of SARS-CoV-2 Infection by Bovine Lactoferrin. BioRxiv, 093781.

Chang, R., Ng, T.B., Sun, W.-Z., 2020. Lactoferrin as potential preventative and treatment for COVID-19. Int. J. Antimicrob. Agents 106118.

Chen, J.M., Fan, Y.C., Lin, J.W., Chen, Y.Y., Hsu, W.L., Chiou, S.S., 2017. Bovine lactoferrin inhibits Dengue virus infectivity by interacting with heparan sulfate, low-density lipoprotein receptor, and DC-SIGN. Int. J. Mol. Sci. 2017 (18), 1957.

Cordeiro, Y., Foguel, D., Silva, J.L., 2013. Pressure-temperature folding landscape in proteins involved in neurodegenerative diseases and cancer. Biophys. Chem. 183, 9–18.

Cutone, A., Rosa, L., Lepanto, M.S., Scotti, M.J., Berlutti, F., Bonaccorsi di Patti, M.C., Musci, G., Valenti, P., 2017. Lactoferrin efficiently counteracts the inflammation-induced changes of the iron homeostasis system in macrophages. Front. Immunol. 8, 705.

Florian, P., Macovei, A., Sima, L., Nichita, N., Mattsby-Baltzer, I., Roseanu, A., 2012. Endocytosis and trafficking of human lactoferrin in macrophage-like human THP-1 cells. Biochem. Cell. Biol. 90 (3), 449–455.

Franco, I., Castillo, E., Pérez, M.D., Calvo, M., Sánchez, L., 2013. Effect of hydrostatic high pressure on the structure and antibacterial activity of recombinant human lactoferrin from transgenic rice. Biosci. Biotechnol. Biochem. 76 (1), 53–59.

Franco, I., Pérez, M.D., Conesa, C., Calvo, M., Sánchez, L., 2018. Effect of technological treatments on bovine lactoferrin: an overview. Food Res. Int. 106, 173–182.

Gerstein, M., Anderson, B.F., Norris, G.E., Baker, E.N., Lesk, A., Chothia, C., 1993. Domain closure in lactoferrin: two hinges produce a see-saw motion between alternative close-packed interfaces. J. Mol. Biol. 234 (2), 357–372.

Hering, N.A., Luettig, L., Krug, S.M., Wiegand, S., Gross, G., van Tol, E.A., Schulzke, J.D., Rosenthal, R., 2017. Lactoferrin protects against intestinal inflammation and bacteria-induced barrier dysfunction in vitro. Ann. N. Y. Acad. Sci. 1405 (1), 177–188.

Hu, Y., Meng, X., Zhang, F., Xiang, Y., Wang, J., 2021. The in vitro antiviral activity of lactoferrin against common human coronaviruses and SARS-CoV-2 is mediated by targeting the heparan sulfate co-receptor. Emerg. Microb. Infect. 10 (1), 317–330.

Jancsó, A., Szunyogh, D., Larsen, F.H., Thulstrup, P.H., Christensen, N.J., Gyurcsik, B., Hemmingsen, L., 2011. Towards the role of metal ions in the structural variability of proteins: CdII speciation of a metal ion binding loop motif. Metallomics 3, 1331–1339.

Jiang, R., Lopez, V., Kelleher, S.L., Lönnerdal, B., 2011. Apo- and holo-lactoferrin are both internalized by lactoferrin receptor via clathrin-mediated endocytosis but differentially affect ERK-signaling and cell proliferation in Caco-2 cells. J. Cell. Physiol. 226 (11), 3022–3031.

Kell, D.B., Heyden, E.L., Pretorius, E., 2020. The biology of lactoferrin, an iron-binding protein that can help defend against viruses and bacteria. Front. Immunol. 11.

Lang, J., Yang, N., Deng, J., Liu, K., Yang, P., Zhang, G., Jiang, C., 2011. Inhibition of SARS pseudovirus cell entry by lactoferrin binding to heparan sulfate proteoglycans. PloS One 6 (8), e23710.

Liu, F., Zhang, S., Li, J., McClements, D.J., Liu, X., 2018. Recent development of lactoferrin-based vehicles for the delivery of bioactive compounds: complexes, emulsions, and nanoparticles. Trends Food Sci. Technol. 79, 67–77.

Lizzi, A.R., Carnicelli, V., Clarkson, M.M., Di Giulio, A., Oratore, A., 2009. Lactoferrin derived peptides: mechanisms of action and theis perspectives as antimicrobial and antitumoral agents. Mini Rev. Med. Chem. 9 (6), 687–695.

Longhi, G., Pietropaolo, V., Mischitelli, M., Longhi, C., Conte, M.P., Marchetti, M., Tinari, A., Valenti, P., Degener, A.M., Seganti, L., Superti, F., 2006. Lactoferrin inhibits early steps of human BK polyomavirus infection. Antivir. Res. 72 (2), 145–152.

Luzi, C., Brisdelli, F., Iorio, R., Bozzi, A., Carnicelli, V., Di Giulio, A., Lizzi, A.R., 2017. Apoptotic effects of bovine apo-lactoferrin on HeLa tumor cells. Cell Biochem. Funct. 35 (1), 33–41.

Majka, G., Śpiewak, K., Kurpiewska, K., Heczko, P., Stochel, G., Strus, M., Brindell, M., 2013. A high-throughput method for the quantification of iron saturation in lactoferrin preparations. Anal. Bioanal. Chem. 405 (15), 5191–5200.

Marchetti, M., Longhi, C., Conte, M.P., Pisani, S., Valenti, P., Seganti, L., 1996. Lactoferrin inhibits herpes simplex virus type 1 adsorption to Vero cells. Antivir. Res. (2-3), 221–231.

Marchetti, M., Superti, F., Ammendolia, M.G., Rossi, P., Valenti, P., Seganti, L., 1999. Inhibition of poliovirus type 1 infection by iron-, manganese- and zinc-saturated lactoferrin. Med. Microbiol. Immunol. 187 (4), 199–204.

Marchetti, M., Trybala, E., Superti, F., Johansson, M., Bergström, T., 2004. Inhibition of herpes simplex virus infection by lactoferrin is dependent on interference with the virus binding to glycosaminoglycans. Virology 318 (1), 405–413.

Mason, P.E., Brady, J.W., Neilson, G.W., Dempseyz, C.E., 2007. The interaction of guanidinium ions with a model peptide. Biophys. J.: Biophys. Lett. 93 (1), L04–L06.

Mata, L., Sanchez, L., Headon, D.R., Calvo, M.J., 1998. Thermal denaturation of human lactoferrin and its effect on the ability to bind iron. Agric. Food Chem. 46, 3964–3970.

Mirabelli, C., Wotring, J.W., Zhang, C.J., McCarty, S.M., Fursmidt, R., Frum, T., Kadambi, N.S., Amin, A.T., O'Meara, T.R., Pretto, C.D., Spence, J.R., Huang, J., Alysandratos, K.D., Kotton, D.N., Handelman, S.K., Wobus, C.E., Weatherwax, K.J., Mashour, G.A., O'Meara, M.J., Sexton, J.Z., 2020. Morphological Cell Profiling of SARS-CoV-2 Infection Identifies Drug Repurposing Candidates for COVID-19. BioRxiv.

Moore, S.A., Anderson, B.F., Groom, C.R., Haridas, M., Baker, E.N., 1997. Three-dimensional structure of diferric bovine lactoferrin at 2.8 A resolution. J. Mol. Biol. 274 (2), 222–236.

Mosmann, T., 1983. Rapid colorimetric assay for cellular growth and survival: application to proliferation and cytotoxicity assays. J. Immunol. Methods 65, 55–63.

Mozhaev, V.V., Heremans, K., Frank, J., Masson, P., Balny, C., 1994. Exploiting the effects of high hydrostatic pressure in biotechnological applications. Trends Biotechnol. 12 (12), 493–501.

Munizaga, T., Gordon, T.A., Carvajal, R.V., Osorio, L.M., Salazar, F.N., Won, M.P., Acuña, S., 2014. Effects of high hydrostatic pressure (HHP) on the protein structure and thermal stability of Sauvignon blanc wine Gipsy. Food Chem. 155, 214–220.

Murphy, M.E., Kariwa, H., Mizutani, T., Yoshimatsu, K., Arikawa, J., Takashima, I., 2000. In vitro antiviral activity of lactoferrin and ribavirin upon hantavirus. Arch. Virol. 145 (8), 1571–1582.

Murphy, M.E., Kariwa, H., Mizutani, T., Tanabe, H., Yoshimatsu, K., Arikawa, J., Takashima, I., 2001. Characterization of in vitro and in vivo antiviral activity of lactoferrin and ribavirin upon hantavirus. J. Vet. Med. Sci. 63 (6), 637–645.

Niether, D., Di Lecce, S., Bresme, F., Wiegand, S., 2018. Unravelling the hydrophobicity of urea in water using thermodiffusion: implications for protein denaturation. Phys. Chem. Chem. Phys. 20 (2), 1012–1020.

Paladini Jr., A.A., Weber, G., 1981. Pressure-induced reversible dissociation of enolase. Biochemistry 20 (9), 2587–2593.

Patel, H.A., Singh, H., Anema, S.G., Creamer, L.K., 2006. Effects of heat and high hydrostatic pressure treatment on dissulfide bonding interchanges between the protein in skin milk. J. Agric. Food Chem. 54, 3409–3420.

Peroni, D.G., Fanos, V., 2020. Lactoferrin is an important factor when breastfeeding and COVID-19 are considered. Acta Paediatr. 109 (10), 2139–2140.

Perrett, S., Zhou, J.M., 2002. Expanding the pressure technique: insights into protein folding from combined use of pressure and chemical denaturants. Biochim. Biophys. Acta 1595, 201–223.

Privalov, P.L., 2009. Microcalorimetry of proteins and their complexes. Methods Mol. Biol. 490, 1–39.

Puri, S., Li, R., Ruszaj, D., Tati, S., Edgerton, M., 2015. Iron binding modulates candidacidal properties of salivary histatin 5. J. Dent. Res. 94 (1), 201–208.

Sabra, S., Agwa, M., 2020. Lactoferrin, a unique molecule with diverse therapeutical and nanotechnological applications. Int. J. Biol. Macromol. 164, 1046–1060.
Schwarcz, W.D., Carnelocce, L., Silva, J.L., Oliveira, A.C., Gonçalves, R.B., 2008. Conformational changes in bovine lactoferrin induced by slow or fast temperature increases. Biol. Chem. 389 (8), 1137–1142.
Serrano, G., Kochergina, I., Albors, A., Diaz, E., Oroval, M., Hueso, G., et al., 2020. Liposomal lactoferrin as potential preventative and cure for COVID-19. Int. J. Res. Health Sci. 8 (1), 8–15.
Silva, J.L., Foguel, D., Royer, C., 2001. Pressure provides new insights into protein folding, dynamics and structure. Trends Biochem. Sci. 26, 612–618.
Silva, J.L., Oliveira, A.C., Vieira, T.C.R.G., Oliveira, G.A.P., Suarez, M.C., Foguel, D., 2014. High-pressure chemical biology and biotechnology. Chem. Rev. 114 (14), 7239–7267.
Singh, I., Swami, R., Pooja, D., Jeengar, M.K., Khan, W., Sistla, R., 2015. Lactoferrin bioconjugated solid lipid nanoparticles: a new drug delivery system for potential brain targeting. J. Drug Target. 24 (3), 212–223.
Sreedhara, A., Flengsrud, R., Prakash, V., Krowarsch, D., Langsrud, T., Kaul, P., Devold, T.G., Vegarud, G.E., 2010. A comparison of effects of pH on the thermal stability and conformation of caprine and bovine lactoferrin. Int. Dairy J. 20, 487–494.
Stanciuc, N., Aprodu, I., Rapeanu, G., Plancken, I., Bahrim, G., Hendrickx, M., 2013. Analysis of the thermally induced structural changes of bovine lactoferrin. J. Agric. Food Chem. 61, 2234–2243.
Superti, F., Agamennone, M., Pietrantoni, A., Ammendolia, M., 2019. Bovine lactoferrin prevents Influenza A virus infection by interfering with the fusogenic function of viral hemagglutinin. Viruses 11 (1), 51.
Suzuki, Y.A., Wong, H., Ashida, K.Y., Schryvers, A.B., Lönnerdal, B., 2008. The N1 domain of human lactoferrin is required for internalization by caco-2 cells and targeting to the nucleus. Biochemistry 47 (41), 10915–10920.
Syed, S.B., Khan, F.I., Khan, S.H., Srivastava, S., Hasan, G.M., Lobb, K.A., Islam, A., Ahmad, F., Hassan, M.I., 2018. Mechanistic insights into the urea-induced denaturation of kinase domain of human integrin linked kinase. Int. J. Biol. Macromol. 111, 208–218.
Torrent, J., Marchal, S., Tortora, P., Lange, R., Balny, C., 2004. High pressure, an alternative approach to understand protein misfolding diseases. Cell. Mol. Biol. 50 (4), 377–385.
van Berkel, P.H.C., Geerts, M.E.J., van Veen, H.A., Kooiman, P.M., Pieper, F.R., De Boer, H.A., et al., 1995. Glycosylated and Unglycosylated Human Lactoferrins Both Bind Iron and Show Identical Affinities towards Human Lysozyme and Bacterial Lipopolysaccharide, but Differ in Their Susceptibilities towards Tryptic Proteolysis Biochemical Journal, 312, pp. 107–114.
Waarts, B.-L., Aneke, O.J.C., Smit, J.M., Kimata, K., Bittman, R., Meijer, D.K.F., Wilschut, J., 2005. Antiviral activity of human lactoferrin: inhibition of alphavirus interaction with heparan sulfate. Virology 333 (2), 284–292.
Wakabayashi, H., Yamauchi, K., Yaeshima, T., Shin, K., Iwatsuki, K., 2008. Recombinant human intelectin binds bovine lactoferrin and its peptides. Biol. Pharm. Bull. 31 (8), 1605–1608.
Wang, B., Timilsena, Y.P., Blanch, E., Adhikari, B., 2017. Lactoferrin: structure, function, denaturation and digestion. Crit. Rev. Food Sci. Nutr. 1–17.